PL-TR-97-2059

DETECTION AND CHARACTERIZATION OF EQUATORIAL SCINTILLATION FOR REAL-TIME OPERATIONAL SUPPORT

W. J. McNeil
A. R. Long
M. J. Kendra

Radex, Inc.
Three Preston Court
Bedford, MA 01730

April 18, 1997

Scientific Report #12

DTIC QUALITY INSPECTED 2

PHILLIPS LABORATORY
Directorate of Geophysics
AIR FORCE MATERIEL COMMAND
HANSCOM AIR FORCE BASE, MA 01731-3010

19970916 152

"This technical report has been reviewed and is approved for publication"

Edward C. Robinson (signature)
EDWARD C. ROBINSON
Contract Manager
Data Analysis Division

Robert E. McInerney (signature)
ROBERT E. McINERNEY, Director
Data Analysis Division

REPORT DOCUMENTATION PAGE

Public reporting burden for this collection of information is estimated to average 1 hour per response, including the time for reviewing instructions, searching existing data sources, gathering and maintaining the data needed, and completing and reviewing the collection of information. Send comments regarding this burden estimate or any other aspect of this collection of information, including suggestions for reducing this burden, to Washington Headquarters Services, Directorate for Information Operations and Reports, 1215 Jefferson Davis Highway, Suite 1204, Arlington, VA 22202-4302, and to the Office of Management and Budget, Paperwork Reduction Project (0704-0188), Washington, DC 20503.

1. AGENCY USE ONLY (Leave Blank)	2. REPORT DATE	3. REPORT TYPE AND DATES COVERED
	18 April 1997	Scientific Report No. 12

4. TITLE AND SUBTITLE

Detection and Characterization of Equatorial Scintillation for Real-Time Operational Support

5. FUNDING NUMBERS

PE 62101F
PR 7659 TA GY WU AA

Contract F19628-93-C-0023

6. AUTHORS

W. J McNeil
A. R. Long
M. J. Kendra

7. PERFORMING ORGANIZATION NAME(S) AND ADDRESS(ES)

RADEX, Inc.
Three Preston Court
Bedford, MA 01730

8. PERFORMING ORGANIZATION REPORT NUMBER

RXR-97041

9. SPONSORING / MONITORING AGENCY NAME(S) AND ADDRESS(ES)

Phillips Laboratory
29 Randolph Road
Hanscom AFB, MA 01731-3010

Contract Manager: Edward C. Robinson/GPD

10. SPONSORING / MONITORING AGENCY REPORT NUMBER

PL-TR-97-2059

11. SUPPLEMENTARY NOTES

12a. DISTRIBUTION / AVAILABILITY STATEMENT

Approved for Public Release
Distribution Unlimited

12b. DISTRIBUTION CODE

13. ABSTRACT (Maximum 200 words)

The Phillips Laboratory Scintillation Network Decision Aid (PL-SCINDA) is a software tool which uses real-time data from remote sites to model ionospheric plasma depletions in the equatorial region. The remote instruments continuously measure S4 from geostationary satellite transmissions. Receivers are currently located in Antofagasta, Chile and Ancón Peru. Different combinations combinations of receiver pairs allow: measurements in eastward and westward directions for each site, drift velocity measurements, and and measurements along the same magnetic field line from receivers at different latitudes. These data are used by the Discrete Scintillation Bubble Model (DSBMOD), an empirical model designed to construct 3-D structures. The spatial extent, motion, and evolution of these structures over time are approximated using real-time data and a priori knowledge of the dynamics of equatorial depletions. The structures are visualized on a Silicon Graphics workstation in OpenGL. Our data allows us to test basic assumptions concerning vertical drift, morphology of depletion structures over long time periods, and bottom-side turbulence versus true plume formation. PL-SCINDA is capable of making short term predictions and issuing short real-time warnings in support of operational users of communications and navigational satellite links. Projection of the outlines of 3-D structures onto a 2-D map for specific satellites allows the generation of custom tailored outage maps for operational users. Routine collection of data is contributing to our understanding of depletion behavior and climatology. . Future plans call for expanding the number of real-time sites, and adding GPS capability.

14. SUBJECT TERMS

Scintillation prediction, Equatorial ionosphere, Ionospheric irregularities, modeling

15. NUMBER OF PAGES

22

16. PRICE CODE

17. SECURITY CLASSIFICATION OF REPORT	18. SECURITY CLASSIFICATION OF THIS PAGE	19. SECURITY CLASSIFICATION OF ABSTRACT	20. LIMITATION OF ABSTRACT
Unclassified	Unclassified	Unclassified	Unlimited

TABLE OF CONTENTS

LIST OF FIGURES

ACKNOWLEDGEMENTS

1. INTRODUCTION

The Phillips Laboratory Scintillation Network Decision Aid (PL-SCINDA) was developed as a "proof of concept" system with the purpose of providing near real-time warning of communication outages due to equatorial spread F (ESF) instabilities [*Kelly*, 1989]. The ESF phenomenon results in plasma density depletions or bubbles in the topside ionosphere. For a detailed discussion see *Aarons and Basu* [1985]. Data is collected at two stations in South America which continuously monitor the scintillation index S_4. These data are periodically down-loaded to Phillips Lab where they are accumulated and quality checked. Files are then shipped to remote sites running the PL-SCINDA software tool. The data are analyzed with the Discrete Bubble Model (DSBMOD) which detects, characterizes, and propagates the depletion bubbles to provide a picture of current outage conditions and to forecast predicted outages for the next few hours. Output from the model consists of three-dimensional depletion bubbles which are mapped along magnetic field lines and which have characteristic top-side heights, time durations, and turbulence strengths and are calculated from the measured S_4 and are dependant on the geometry of the station and satellite link where the measurement was made. A data-driven model of the anomaly crest is used to predict the scintillation level along the latitudinal extent of the bubble and a phase screen model [*Rino*, 1979] is used to compute the equivalent S_4 for arbitrary ground station and satellite pairs.

The model results are displayed and manipulated by a visualization tool incorporating several options of operational significance. The tool has full ephemeris capability for any satellite in the current data base. Bubbles are displayed in three dimensions along with selected ground station to satellite links, and continental outlines or a surface photograph are rendered for orientation. Links are colored to indicate outage conditions. In addition to the real-time capability, the tool has a play-back option for anomaly analysis. Two-dimensional maps can also be generated showing ground projections of the bubbles with S_4 index computed for a chosen satellite and frequency. The 2-D maps can be projected ahead in time up to a maximum of three hours to show the predicted outages at future times. Hard copy of these maps suitable for facsimile transmission can be generated in support of mission operations. To provide global coverage and to forecast when scintillation has not been observed or data is not available, the tool displays the predictions of the Wideband Model WBMOD [*Secan, et al.*, 1995]. This version of WBMOD is itself driven by real-time scintillation data, where available.

The two sensors now in place have been operational for more than a year. Climatological information gathered from the rather unique configuration is currently being analyzed and is expected to contribute to our understanding of equatorial ionospheric irregularities. The system is currently being expanded to provide coverage in regions of military significance and to investigate the global behavior of scintillation. We have installed GPS scintillation units at the South American sites and are developing algorithms for including these in the model. Plans are for expansion both to the Pacific and the Middle East in the upcoming year.

1

2. DATA COLLECTION

The present configuration consists of two receivers located in Antofagasta, Chile and Ancón, Peru. Both receivers are tuned to a 250 MHz geosynchronous satellite at 99° W longitude and another at 23° W longitude measuring UHF scintillation. They are also tuned to the GOES-8 satellite which is approximately overhead, providing scintillation measurements in the L-band. The locations were chosen so that the ionospheric penetration points of the westward link at Antofagasta and the eastward link at Ancón lie approximately along the same field line. Measurements at Ancón are about 1° above the magnetic equator and those from Antofagasta are about 11° below, near but somewhat north of the usual anomaly crest. The separation in longitude of the penetration points allow for observation of longitudinal variations in climatology and of the time evolution of plume structures. Taken together, the configuration covers about 12° in longitude from about 66° to 78° W. Figure 1 shows a schematic of the UHF links currently employed by PL-SCINDA, including the 300 km penetration points.

SCINTILLATION NETWORK DATA COLLECTION

► REAL TIME S4 AND DRIFT VELOCITY EVERY 87 SECONDS FROM SUNSET TO DAWN
► DATA TRANSFERRED TO PHILLIPS LABORATORY EVERY 15 MINUTES

ANCON, PERU
11.83 S, 77.17W

ANTOFAGASTA, CHILE
22.44 S, 70.50W

S4 AND DRIFT VELOCITY MEASURED
AT THE IONOSPHERE PENETRATION
POINTS, ALTITUDE = 300 km

FY-97:
► INCORPORATE GPS L-BAND CAPABILITY
► ADD MIDDLE EAST STATIONS
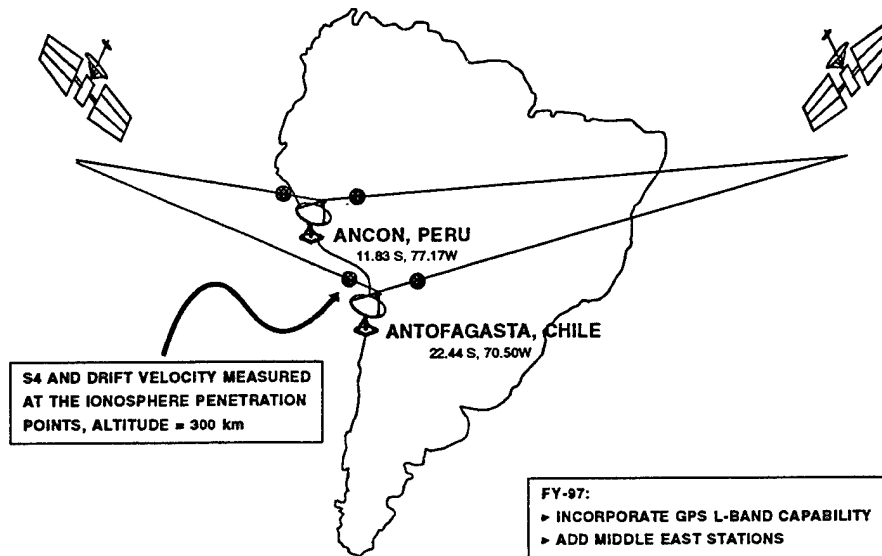
Figure 1. Schematic diagram of receiver locations and ionospheric penetration points for the current configuration.

Measurements are made throughout the night and throughout the year. On-site processors compute an S_4 value for each link about once per minute and one-half. Redundant measurements from antennae displaced about 100 meters to the east are used to calculate the eastward drift of the ionosphere, providing a drift velocity at the same frequency. Typical scintillation data are shown in Figure 2.
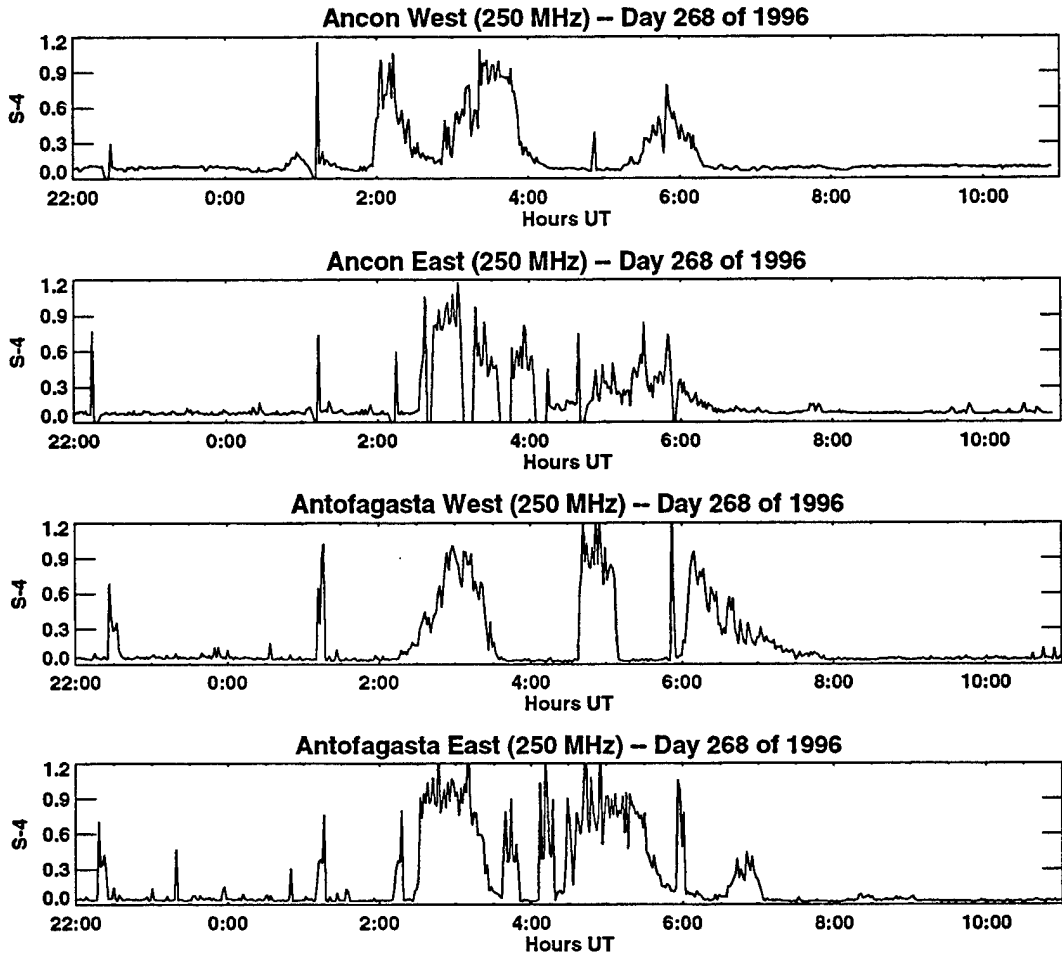
Figure 2. Sample scintillation data from the four links comprising the current scintillation bubble model.

The data exhibits numerous noise spikes and dropouts. It is not entirely clear whether structures like the ones on either side of 4:00 Z at Antofagasta East constitute real scintillation or not. Spikes like the ones around 1:00 Z are more clearly the result of satellite or station operations. The S_4 data are subjected to a filter which attempts to differentiate between true ionospheric events and noise spikes. The filter requires several points to one side or the other of an S_4 value to remain above a chosen threshold. Otherwise, the point is removed. The filter also extends scintillation over data dropouts by extrapolating for a period of time up to one-half hour.

3

The data in Figure 2 shows several well-defined plumes and other features that are not so well-defined. On this particular night, scintillation begins at Ancón West and is picked up at Ancón East about one-half hour later. The onset down-field at Antofagasta West is more gradual than at Ancón East, indicating that this plume is in the process of developing. Differentiation between developing and fully developed plumes is done at the links along the common field line, but additional assumptions must be added at the other two links. Comparing the common field line data, Ancón East and Antofagasta West, we see another remarkable feature. From about 2:30 Z to 3:30 Z, there is scintillation at both links of about the same magnitude. However, from 3:30 Z to 4:30 Z, scintillation ceases at Antofagasta but persists at Ancón. Later, around 5:00 Z there is strong scintillation at Antofagasta, but that at Ancón is now much weaker. This indicates a change in the latitudinal dependence of the scintillation over the course of the night. These are examples of the complexities that must be addressed in the modeling.

At the stations, individual measurements are combined into running three-hour files. This provides some redundancy in case of transmission failure. At fifteen minute intervals, these three-hour files are obtained through the internet by a cron running on a Sparc 10 at PL. The three-hour files from each station are consolidated into nightly files and are disseminated to workstations running PL-SCINDA, again through the internet. At this point, recent orbital elements and near real-time geophysical parameters are added to the data base, so that a single transmission is sufficient to update the system with all required parameters. Orbital elements are obtained weekly from the Air Force Institute of Technology and geophysical parameters from the Space Environments Laboratory. The geophysical parameters are not currently used by DSBMOD, but are displayed by the visualization tool and are used to drive the WBMOD climatology.

3. THE BUBBLE MODEL

The scintillation data are introduced into the Discrete Scintillation Bubble Model (DSBMOD) which attempts to extend the information garnered from the stations over the entire theater, extrapolating both spatially and forward in time for forecasting. The S_4 values are averaged over five minute intervals, then normalized by computing an equivalent S_4 for an equatorial station located at Ancón and viewing a geosynchronous satellite at an elevation of 45° to the east. This normalization compensates for the various elevations and angles relative to the geomagnetic field of the measured links. Added to the measured S_4 observed throughout the night are measured ionospheric drift velocity and several assumptions about scintillation bubble formation, evolution, and destruction. These assumptions include the rate of growth of the bubble topside, the rate of decay of the turbulence strength parameter C_kL, and the latitude dependence of the scintillation strength. The last of these is modeled from the observed scintillation along the common field line. The generation and destruction of bubbles detected at the four station-to-satellite links is governed by rules which are different for each link. While the better part of the model can be applied to any set of receivers and satellites, these rules are specific to the current configuration.

3. 1 BUBBLE RECOGNITION

Bubbles are generated by examining the S_4 data from each of the four links from sunset up to the present time. A bubble is created whenever two consecutive 5-minute S_4 values are encountered above a set threshold. A bubble is terminated whenever two points below the threshold are obtained. If scintillation persists above the threshold at a particular link for more than one-half hour, the current bubble is terminated at the half-hour and a new bubble is begun. This technique allows for longitudinal variations in the modeled S_4 since each bubble is assigned an individual turbulence strength. Bubbles lasting less than fifteen minutes are discarded. This is an additional technique for differentiating between scintillation structures and noise. Figure 3 shows the discrete bubbles that were generated from the data taken on Day 268 of 1996 along with the five-minute normalized S_4 values.
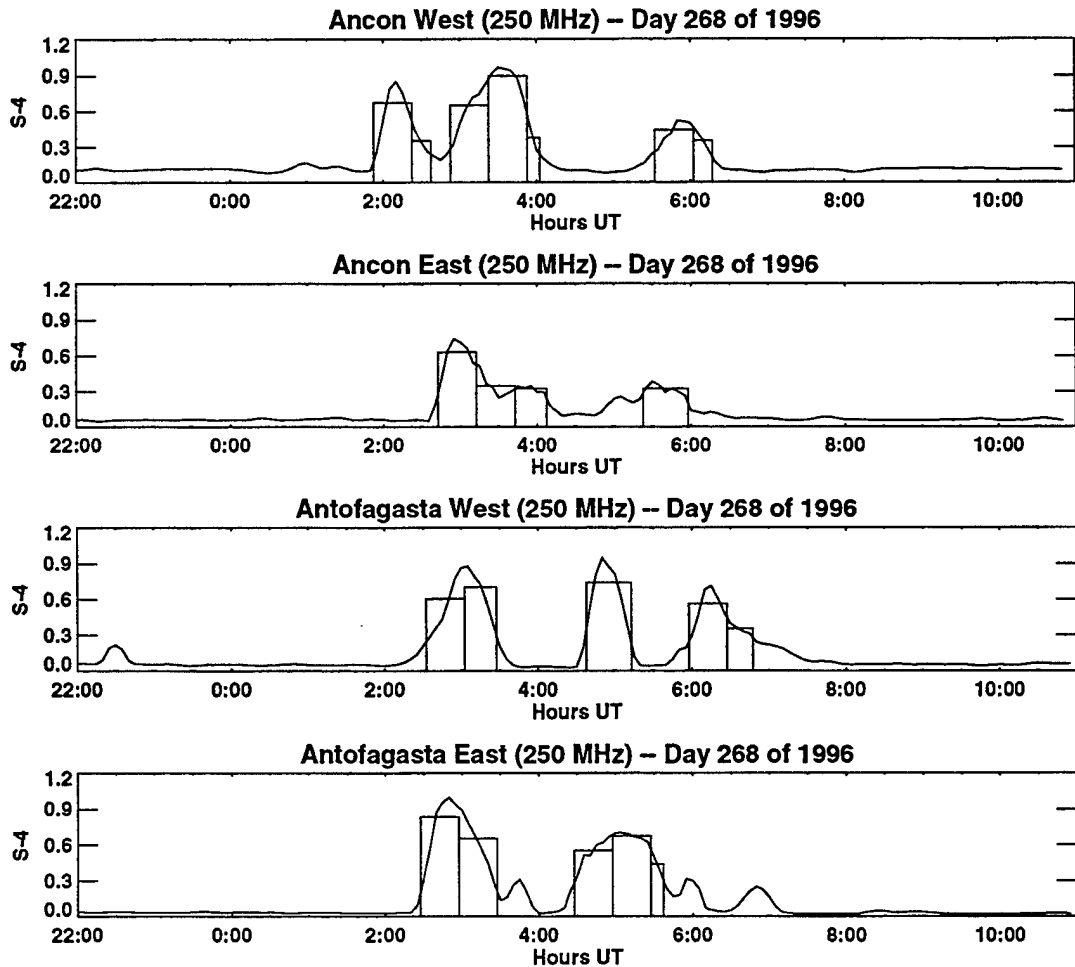
Figure 3. Edited and averaged S_4 data along with the bubbles generated from the night shown in Figure 2.

5

The figure illustrates how scintillation is allowed to vary over the course of a single event by the half-hour limit for any particular bubble duration. It is clear in the smoothed data that the boundary between scintillation periods is not sharp in most cases. We have chosen to represent the bubbles as periods of constant C_kL for the sake of simplicity in the subsequent computations and display. The threshold recognition, coupled with the duration requirement for isolated bubbles, leads the model to ignore the features at 3:30 Z and at and after 6:00 Z at Antofagasta East. The first two of these are the result of somewhat dubious spikes and all are, after averaging, below what is considered to be significant scintillation. For UHF communications warnings are issued when S_4 reaches a value of 0.3. Whether or not events below this level are retained or discarded in the data is therefore not important.

3.2 BUBBLE PROPAGATION

Once detected, bubbles are propagated forward from the time of detection to the present time or to the time for which an outage projection is desired. Bubbles emanate from the penetration points of the respective links and move eastward with the modeled ionospheric drift velocity. Bubbles are characterized by a topside altitude at the magnetic equator and by a longitudinal extent. The initial and final topside altitude of a bubble depends on the link from which the bubble originates. Bubbles are assigned an initial topside altitude and allowed to grow upward at a rate of 50 m/s based on the age of the bubble. However, bubbles that are simply continuations of previous half-hour segments grow according to the first bubble in the segment. Bubbles from Ancón begin with an equatorial topside of 350 km and bubbles from Antofagasta begin at 450 km in order to put the bottom edge of the bubble at the Antofagasta penetration points. Bubble shapes are computed along the field line intercepting the magnetic equator at the topside altitude and the geographic longitude of the bubble. The bottom side of the bubble is taken to be 300 km regardless of the bubble age. Bubbles grow to a maximum of 1,000 km for the purpose of field line tracking. However, the maximum height of any point in a bubble is limited to 650 km for display and for computation of the outages. This empirical restriction limits the region of scintillation to between 300 and 650 km, regardless of the height of the depletion.

Bubbles from Ancón West are allowed to grow and travel eastward until they come to the penetration point for Ancón East (equals Antofagasta West). There, they are destroyed since this scintillation, if it has not died away, should be picked up in the eastward link. Bubbles from Ancón East are generated at the link and move eastward, but grow only to a maximum topside of 400 km. This puts the bottom edge of the bubble a degree or two north of the Antofagasta West link. These are used to represent bottom side turbulence that does not develop into full-sized plumes. Plumes generated at Antofagasta West will occupy the same geographic area but will appear overtop the bubbles from Ancón East. Antofagasta West bubbles grow and drift eastward to the Antofagasta East link, where they are destroyed. Bubbles generated at Antofagasta East grow and drift and persist until sunrise. After local midnight, bubble topsides are gradually increased so that all bubbles (except those from Ancón East) achieve the maximum topside altitude. This represents the assumption that late night plumes are more or less fully developed.

6

An example of an early night bubble configuration is shown in Figure 4. There, the dark region is used to represent S_4 above the "red" level of 0.6, and the lighter shading represents scintillation above the "yellow" level of 0.3.

Discrete Bubble Model 96/269 at 03:00:00 Zulu
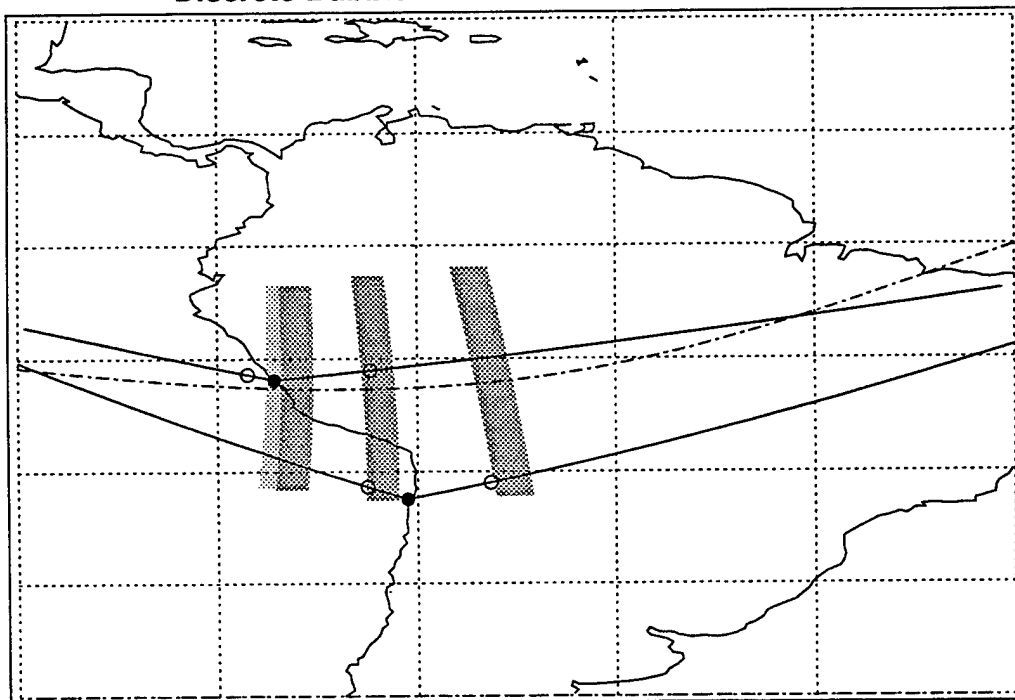
Figure 4. Bubbles from the early evening of Day 268. Dark shading represents $S_4 > 0.6$ and light represents $S_4 > 0.3$.

In the figure, bubbles are being produced from all four links. The bubble from Ancón East has been removed, however, because it would have fallen underneath the bubble from Antofagasta West. The shading of the bubbles represent the S_4 values calculated for the hypothetical satellite at 250 MHz to the west of Ancón at 45° elevation. The bubbles from the two Antofagasta links are approximately the same age and therefore the same size. These are links which are currently scintillating at the time of the figure. The two bubbles from Ancón West represent the same scintillation event which was broken in two after the first half hour. The average S_4 values in the two segments are different. The forward bubble is above the red threshold and the smaller bubble following it is below this threshold but above the yellow threshold. The bubbles have broken off from Ancón since the scintillation has ceased at about 3:00 Z, or at least have fallen below the threshold for bubble recognition. Actually, looking back at Figure 3, there is scintillation above the threshold at 3:00 Z, but the required two 5-minute periods have not yet been observed. At least ten minutes of scintillation is required to generate a bubble. To this is added up to fifteen minutes delay in obtaining the data, since the data is shipped at fifteen minute intervals. This means that in real time operation, a bubble will appear within one-half hour after scintillation is first detected.

Figure 5 shows the bubbles one hour later. First bubbles from Ancón West have grown high enough to pass over the penetration point of the Antofagasta West link. However, scintillation is not currently being observed from Antofagasta West. The Ancón West bubbles are being destroyed at the Antofagasta West penetration point. Ancón East is currently scintillating, however, and a bubble is being generated from the link. The bubble is restricted in size so that it will never grow large enough to reach Antofagasta. It seems probable that the initial bubble from Ancón West did not grow after all. Having no information down-field to the west of Antofagasta West, however, we allowed it to grow then corrected the situation from the observation at Ancón East.

Discrete Bubble Model 96/269 at 04:00:00 Zulu
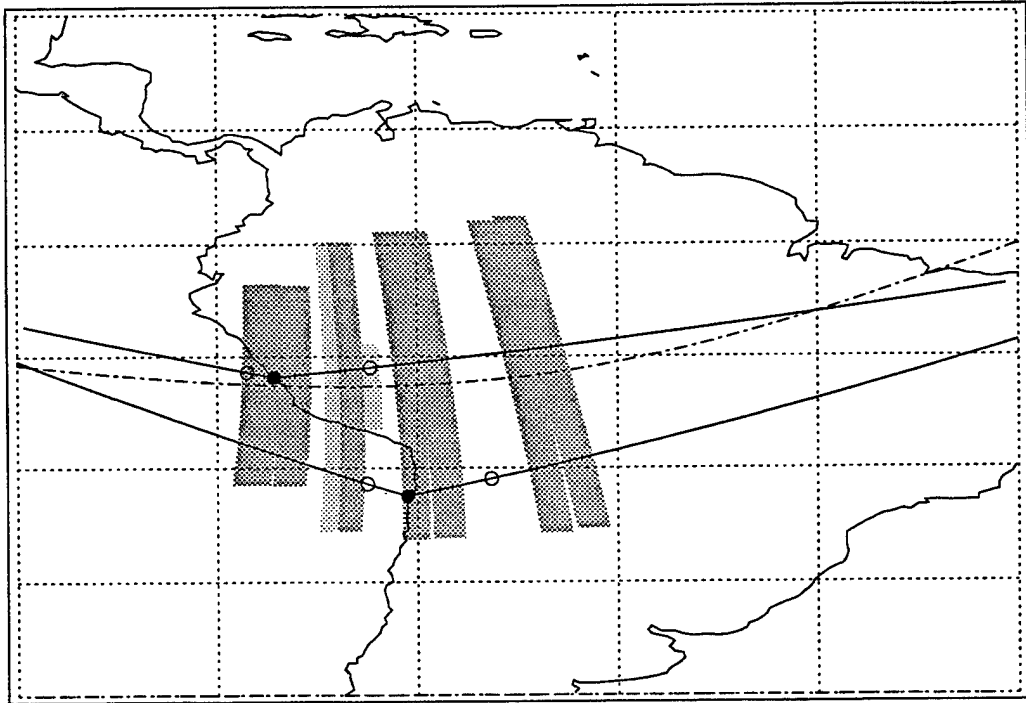
Figure 5.   The discrete bubble model evaluated at 4:00 Z.

Although not apparent from Figures 4 and 5, scintillation in the bubbles does vary with latitude. The latitudinal dependence is derived from the WBMOD model [*Fremouw and Bates*, 1971] which is driven by the observed latitude dependence along the common field line links. The average values of S_4 observed during the night are used to adjust the equatorial and crest of C $_k$ L. This functional form is then used to scale the measured $C_k L$ along each bubble. The functional form changes during the night as more observations are added to the average. The bubbles in Figures 4 and 5 have essentially no latitude variation in $C_k L$ up to the edge of the anomaly region, about $20°$ from the magnetic equator. This is because the data up to 4:00 Z shows pretty much the same magnitude of scintillation at both Ancón and Antofagasta. Later in the night, the equatorial scintillation becomes weaker than that at Antofagasta, and the latitude dependence changes accordingly.

Figure 6 shows the model later in the night. All bubbles are now fully developed and extend to the maximum magnetic latitude modeled, which is about 20° above the equator. They have acquired a latitude dependence characterized by lower level of scintillation intensity at the equator and a peak at the anomaly crest.

**Discrete Bubble Model 96/269 at 07:00:00 Zulu**
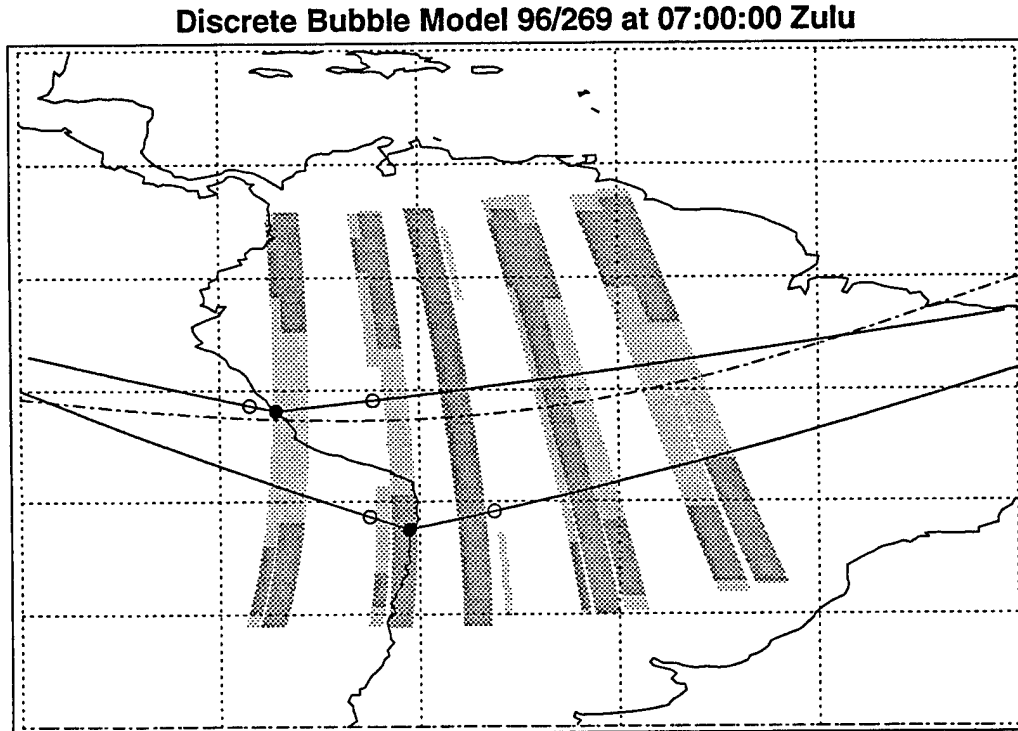
Figure 6. Bubbles from DSBMOD near the end of the night.

Also apparent from comparing Figures 5 and 6 is that the scintillation intensity of the older bubbles has decreased. The model assumes a decay beginning three hours after a bubble is first detected and reducing the value of C_kL by $1/e$ in the following hour. This behavior is somewhat *ad hoc* but represents, at least, the fact that the model is not expected to be accurate in predicting scintillation for a time span of more than three to four hours.

The model attempts to predict the future configuration of bubbles based on the data currently available. This projection is done by first generating all bubbles as usual from past data and moving them to their positions at the present time. They are then projected forward based on an empirical model for the drift velocity and are allowed to grow as usual. Bubbles are not destroyed if they reach a subsequent link between the current time and the time of the prediction, but rather are allowed to drift over the links to the east of where they were created. Stations scintillating at the current time are assumed to stop. This means that the region from Ancón's western link to the trailing edge of the western-most bubble will not be covered by the model. It is instructive to compare the model's predictions with the observed bubbles. One such comparison is made in Figure 7, which shows extrapolation of the data taken up to 4:00 Z forward in time to 7:00 Z, a

three-hour prediction. This is to be compared to the bubbles in Figure 6 which were generated using all the data up to 7:00 Z. Predicting outages in advance is a primary task of the model, and considerable attention has been given to the design in this respect.

Bubbles from 4:00 Z extrapolated to 7:00 Z
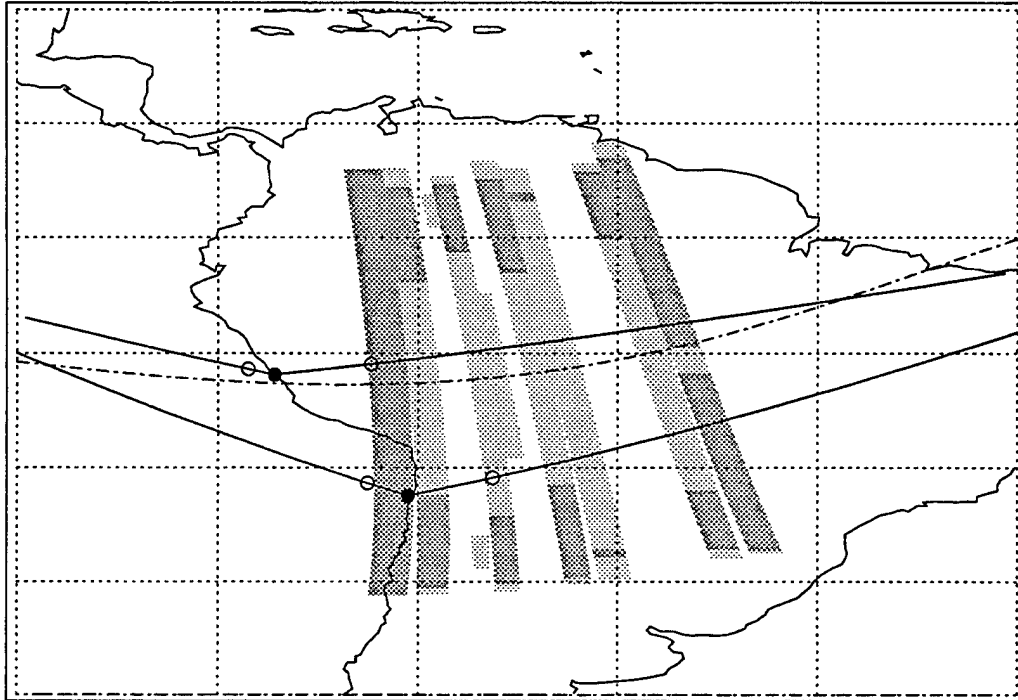
Figure 7. Predicted bubble positions at 7:00 Z using data from three hours before.

In making the comparison, it should be noted that a three-hour projection is about the limit of the model accuracy. This is due mainly to the fact that a bubble maintains its integrity only for a few hours at most. Therefore, prediction past a three-hour limit is not expected to be very good. Even so, the comparison is not unfavorable. The bubble between Ancón and Antofagasta has been missed entirely, since it was not detected at 4:00 Z. However, the other four bubbles are more or less in the correct position. The predicted scintillation directly over Antofagasta and at the eastern link is in fact observed. It is important to note that in Figure 7, all bubbles except the last one to the east are based on scintillation measured at links to the west. Looking back at Figure 4 should clarify this point. In Figure 6, the central three bubbles have been recently detected by Antofagasta East or West. The intensities of scintillation agree somewhat less well with the predictions, due mostly to changes in the model of the latitude dependence with the addition of the extra three hours of data. We are presently in the process of evaluating the model over a large data set and are attempting to refine and fine tune the predictive capabilities. Overall, though, the behavior at this point is quite satisfactory.

3.3 OUTAGE CALCULATIONS

The examples of the model results shown so far are projections of the bubbles in latitude and longitude. These are of limited usefulness for operations. A more useful product is what we call an outage map. This shows the predicted scintillation level at all geographic locations for a predicted set of bubbles and a chosen satellite. The S_4 values are computed with the phase screen model [*Rino*, 1979] including the full geometry of the location to satellite link and the magnetic field effects. Frequency is also included in this computation, although the power law dependence employed for S_4 is truly valid only in the UHF range.

RTS-2 Scintillation Outage Model 96/269 at 05:00:00 Zulu
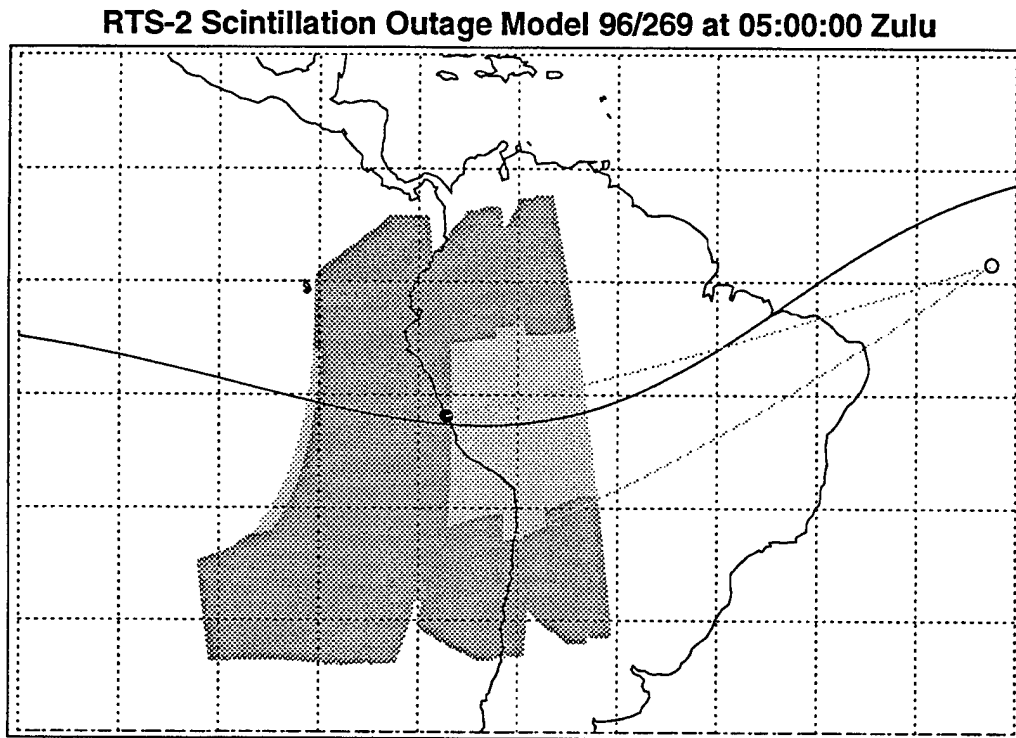
Figure 8. Sample outage map computed for the easterly satellite at 250 MHz. Dark shading indicates $S_4 > 0.6$ and light $S_4 > 0.3$.

Because of the geometric effect, the outage region occupies a substantially larger area than do the bubbles themselves. These "shadows" become larger as the satellite moves nearer the horizon. The decrease in the slant angle at the penetration point also leads to an increase in the computed S_4 as does the increase in angle between the ray path and the magnetic equator. These effects magnify the longitudinal dependence assigned to the bubbles. One also sees that, although the bubbles themselves are discrete, the outage region generated from them is continuous at the equator and at the southern station. The model can generate outages for arbitrary satellites and the calculation extends all the way to the edge of the satellite footprint, the edge of which can be seen at the lower left of Figure 8.

11

4. THE VISUALIZATION TOOL

To support the model at the operational level, an interactive viewer has been developed using OpenGL graphics software on Silicon Graphics workstations. The tool consists of a 3-D window for viewing the scintillation bubbles and a 2-D window for display of the outage maps. The 3-D window is shown in Figure 9.
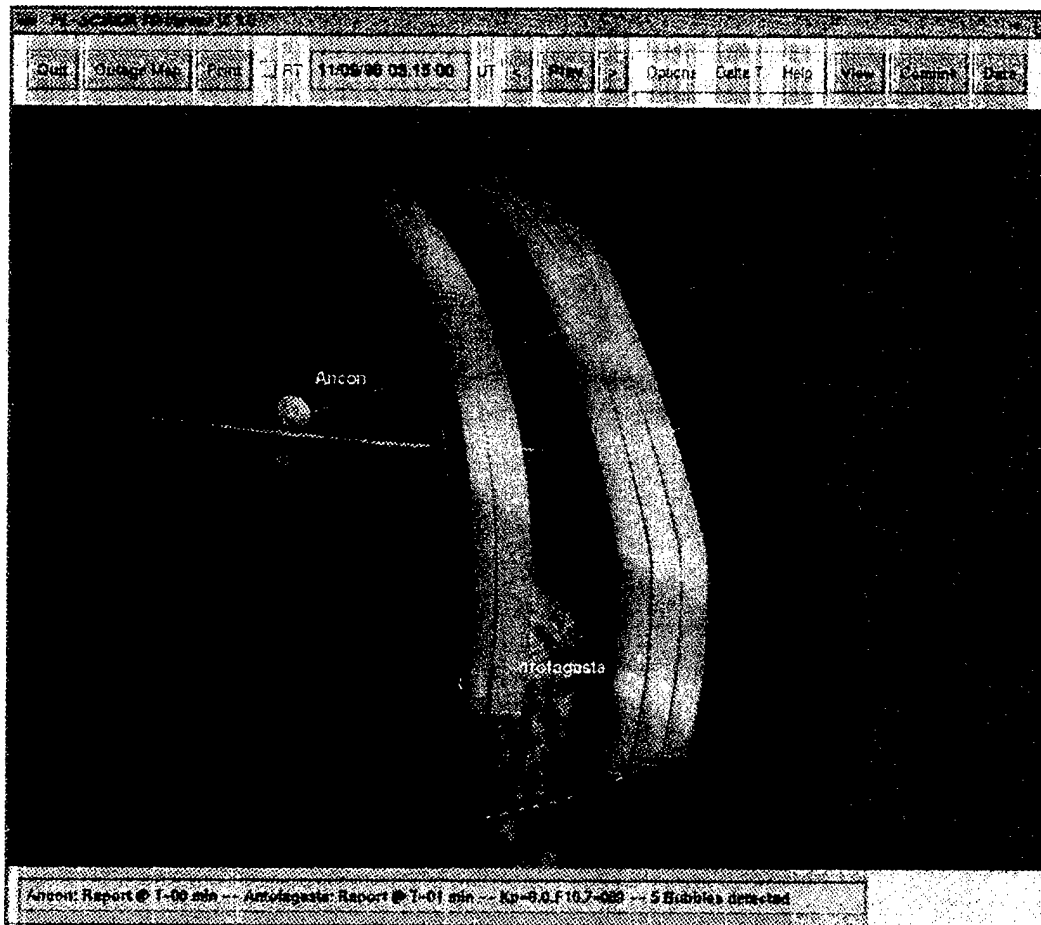
Figure 9. Sample of the PL-SCINDA main window showing bubbles and satellite to station links.

There are three sections to the window. The control area across the top gives the user control over the time and region of the world to display and includes buttons to initiate the pull-down menus. Controls also allow the user to switch between real-time mode or a playback mode which allows any available prior data to be displayed. The display area in the center shows a section of the earth with chosen satellite links to ground stations. The bubbles are displayed in either red or yellow to indicate user-selected thresholds for moderate and severe scintillation. The bottom line of the display reports the status of the station reports and gives the present values of K_p and Sunspot Number.

The "Data" button brings up a screen which displays the scintillation data, bubbles, and measured drift velocities in windows similar to Figure 3. The "Comlink" button brings up a control panel that allows the user to specify arbitrary satellites and ground stations and to set frequencies. The thresholds represented by the bubbles in the 3-D window correspond to normalized S_4 from the "standard link" defined earlier. They correspond to UHF scintillation at 250 MHz. This makes sense because in 3-dimensions, the geometric effects, and therefore the scintillation index, are different for different stations and satellites. To find the actual S_4 for a particular link, the user generates an outage map for the region and satellite of interest.
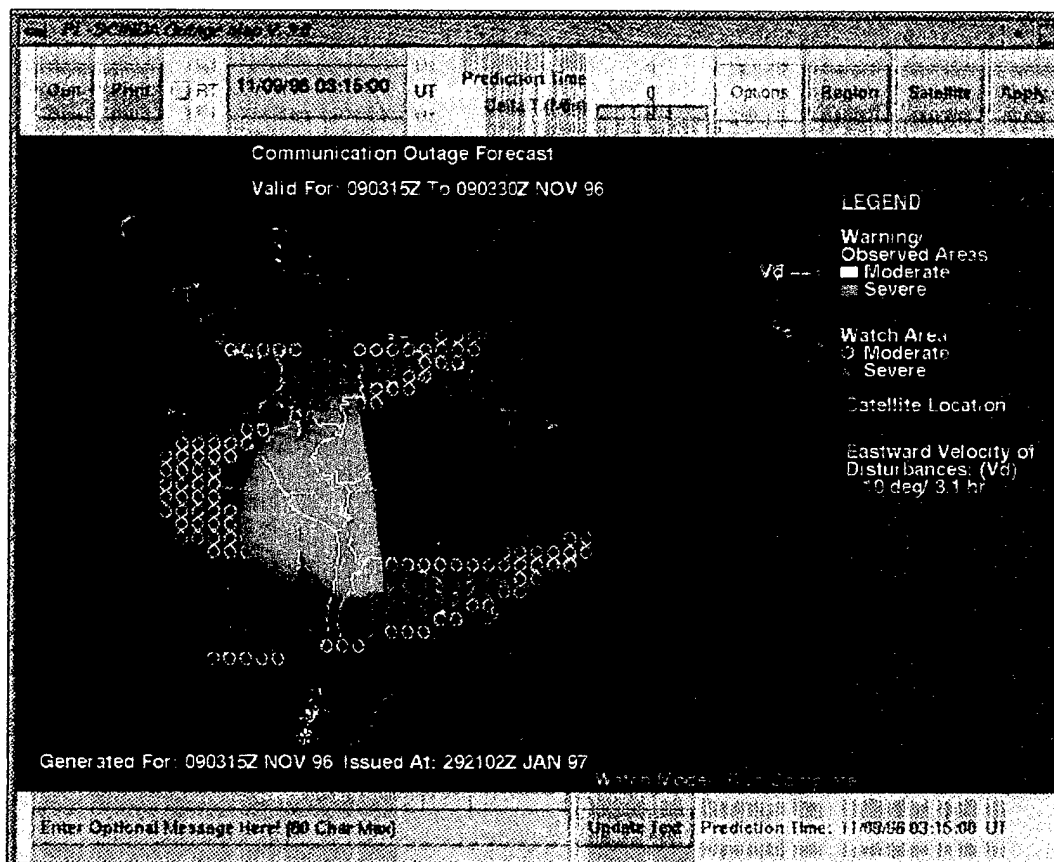
Figure 10. Sample of the PL-SCINDA outage map window.

A sample outage map is shown in Figure 10. The window has the same three basic regions as the 3-D window. The time control widget allows the user to vary the time for the display. There is also a slider to show predictions ahead in time. By the use of multiple windows, the user can easily compare the predictions of the model to the model evaluated with data from further ahead in time. The display shows moderate and severe predicted scintillation calculated from the bubbles, as described earlier. In addition, the results of the WBMOD model are displayed evaluated for the same satellite and frequency.

13

The primary operational product from the system is an outage map pretty much identical to the display window in Figure 10. This is produced in either GIF or PostScript format and the hard-copy version is suitable for facsimile transmission. We envision that these maps could be generated at a central site and sent *via* telephone or internet to the field. We are also exploring versions of PL-SCINDA which could run on lap-top SUI workstations or on a PC. These could operate independently in the field. From its conception, both the modeling and the display tool have been tailored to operational support.

5. SUMMARY

The PL-SCINDA scintillation detection, modeling, and warning system has been designed to provide a valuable asset to military operations, addressing the important concerns of geophysical outages in GPS positioning and UHF ground and satellite communications. The model detects outages from ground stations and relays these data to a central site where the data is then collected and sent out to workstations running PL-SCINDA. The model then analyzes the scintillation and uses measured ionospheric drift, along with empirical assumptions about scintillation plumes, to extrapolate the information over an area surrounding the sensors. The information is then projected forward in time, again using drifts and some assumptions. A visualization tool has been developed to allow the user quick and easy access to the information. Throughout a year of operations, we have found that this concept is indeed workable, and have found that the extrapolation and projection of these plumes can be accomplished with quite reasonable reliability. The project has attracted substantial interest and expansion is now underway, both to GPS applications and to other operational sites.

REFERENCES

Aarons, J. and S. Basu, Scintillation on Transionospheric Radio Signals, in *Handbook of Geophysics and the Space Environment*, A. S. Jursa, ed., AFGL/AFSC/USAF, 1985, AFGL-TR-85-0315, ADA167000.

Fremouw, E. J. and J. F. Bates, Worldwide behavior of average UHF-UHF scintillation, *Radio Sci.*, **6**, 863, 1971.

Kelly, M. C., *The Earth's Ionosphere. Int. Geophys. Ser.*, vol. 43, p. 71, Academic, San Diego, Calif., 1989.

Rino, C. L., A power law phase screen model for ionospheric scintillation, *Radio Sci.*, **14**, 1135, 1979.

Secan, J. A., R. M. Bussey, and E. J. Fremouw, An improved model of equatorial scintillation, *Radio Sci.*, **30**, 607, 1995.